

Portraying the Impact of the Tibetan Plateau on Global Climate

HAIJUN YANG, XINGCHEN SHEN, JIE YAO, AND QIN WEN

*Laboratory for Climate and Ocean–Atmosphere Studies and Department of Atmospheric and Oceanic Sciences,
School of Physics, Peking University, Beijing, China*

(Manuscript received 29 October 2018, in final form 18 September 2019)

ABSTRACT


As the most extensive highland in the world, the Tibetan Plateau (TP) plays an important role in shaping the global climate. Quantifying the effect of the TP on global climate is the first step for a full understanding of the TP's standing on planet Earth. Through coupled model sensitivity experiments, we draw a panorama of the TP's global impact in this paper. Our model results show that the absence of the TP would result in a 4°C colder and 10% drier climate in the Northern Hemisphere (NH). The TP has a striking remote effect on the North Atlantic. Removing the TP would enhance the westerlies in the mid- to high latitudes of the NH and weaken the easterlies over the tropical Pacific. More moisture would be relocated from the tropical Pacific to the North Atlantic, shutting down the Atlantic thermohaline circulation, which would eventually result in more than 15°C colder and 20% drier climate over the North Atlantic. Our model results suggest that the presence of the TP may have contributed greatly to the hospitable modern climate in the NH, by promoting the establishment of the thermohaline circulation in the Atlantic, and therefore enhancing the northward ocean heat transport and atmosphere moisture transport across the equator.

1. Introduction

The Tibetan Plateau (TP) is located over the Eurasian continent, having a total area of about 2.5 million square kilometers in the region of 25°–40°N and 70°–105°E, and an average elevation of about 4000 m (Fig. 1). As the highest and most extensive highland in the world, the TP plays a crucial role in the formation of modern climate in the Northern Hemisphere (NH) (Yeh et al. 1957; Yeh and Gao 1979; Yanai et al. 1992; Meehl 1994; Wu et al. 1997, 2007, 2012a,b; Wu 2004; Yao et al. 2006, 2012; Cheng and Wu 2007; Duan and Wu 2008). Particularly, the TP exerts enormous impact on weather and climate in Asia (Kutzbach et al. 1989; Boos and Kuang 2010; Wu et al. 2012a,b, 2015). During summertime, the TP acts like a huge heat engine, enhancing the Asian summer monsoon and precipitation over East Asia (Kutzbach et al. 1989; Yanai et al. 1992; Duan and Wu 2005; Wang et al. 2005; Wu et al. 2012b, 2015; Gao et al. 2013). During wintertime, the existence of the TP enhances the winter cold air break from the Siberian high, which can

potentially increase the spring persistent rainfall south of the lower reaches of the Yangtze River, and the premonsoon precipitation over South China (Wu et al. 2005).

The fundamental role of the TP in the formation of modern climate can be understood from the paleoclimatic record. The uplift of the TP began about 50 Ma (million years ago), and was accelerated about 10–8 Ma or more recently (Harrison et al. 1992; Molnar et al. 1993), which has pushed the establishment of the monsoon system in East Asia (Ruddiman and Kutzbach 1989; Kutzbach et al. 1993; An et al. 2001). Accompanying the rapid orographic change, Asian climate experienced enhanced aridity in its interior and the onsets of both the Indian and East Asian monsoons about 9–8 Ma (An et al. 2001). The intensification of the East Asian summer and winter monsoons had lasted for about 5 million years, together with increased dust transport to the North Pacific Ocean (An et al. 2001). The accumulated dust over the Pacific could have resulted in more precipitation and low clouds by providing more nuclei of condensation to the atmosphere, leading to freshening and cooling of the North Pacific (Rea et al. 1998). Paleoclimatic evidence shows a possible strong North Pacific Deep Water (NPDW) formation between 70 and 30 Ma and a diminishing NPDW since 30 Ma. The

 Denotes content that is immediately available upon publication as open access.

Corresponding author: Haijun Yang, hjyang@pku.edu.cn

DOI: 10.1175/JCLI-D-18-0734.1

© 2020 American Meteorological Society. For information regarding reuse of this content and general copyright information, consult the [AMS Copyright Policy](https://www.ametsoc.org/PUBSReuseLicenses) (www.ametsoc.org/PUBSReuseLicenses).

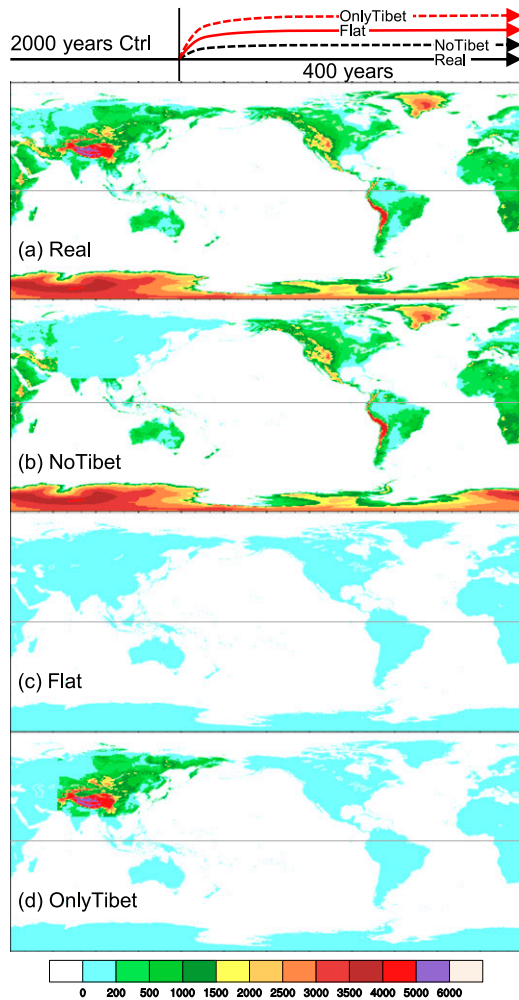


FIG. 1. Topography configuration in coupled model experiments: (a) the control experiment with realistic topography (Real), (b) the experiment without the Tibetan Plateau (TP; NoTibet), (c) the experiment with global flat topography (Flat), and (d) the experiment with Tibetan topography only (OnlyTibet). The topmost panel shows the integration lengths of these experiments.

NPDW has nearly disappeared since 10 Ma (Ferreira et al. 2018, and references therein), and the timing is consistent with that of the rapid TP uplift. Therefore, the TP may have played a critical role in shaping the modern climate, particularly the modern ocean circulation.

Some coupled modeling results have shown that present-day configuration of mountains is an important background to the modern-state ocean thermohaline circulation (i.e., deep water formation in the North Atlantic). Such deep water formation would have occurred in the Pacific in a flat world (Schmittner et al. 2011; Sinha et al. 2012). Fallah et al. (2016) and Su et al. (2018) further pointed out that removing the TP can lead to a collapse of the Atlantic thermohaline circulation. Using different models, different researchers show a similar

concept that continental mountains can affect the state of thermohaline circulation to a great extent. However, the mechanisms proposed in these studies are very different. For example, Schmittner et al. (2011) showed that it is the Rocky Mountains that block water vapor transport from the North Pacific to the Atlantic Ocean, contributing to the increased salinity and deep water formation in the Atlantic. For the mechanism of the weakening Atlantic thermohaline circulation in response to the TP removal, Fallah et al. (2016) emphasized the role of reduced northward ocean heat transport from the tropical Atlantic, while Su et al. (2018) noted the critical role of northward atmospheric moisture transport over the North Atlantic. The discrepancies in mechanisms suggest the complexity of the TP's role in affecting global ocean circulations. More coupled modeling studies are needed.

Despite numerous observational and modeling studies on the TP, there is still a lack of a panoramic view of the TP's global impact. We intend to quantify the effect of the TP on global climate using a unified coupled climate model. This is much needed because on the one hand the ecosystem of the TP region is fragile and very sensitive to current global warming, and on the other hand the changes over the TP region would have profound feedback to the global climate. Observations have shown that during the past half century, the warming rate around the TP region was about $0.35^{\circ}\text{C decade}^{-1}$ (Xu et al. 2017), 3 times of that of the global-mean surface temperature. Therefore, we need to address a very fundamental question first: how different would the global climate be without the TP?

This work is our first step to fully recognize the TP's role in Earth climate. Through sensitivity experiments using a coupled Earth system model, we quantify the impact of the TP on the global overall climate. By comparing the climate in a realistic world and that in a world without the TP, we demonstrate that the presence of the TP would result in a 4°C warmer and 10% wetter climate in the NH. Without the TP, more moisture would be relocated eastward from the tropical Pacific to the North Atlantic, shutting down the Atlantic thermohaline circulation, which can eventually result in more than 15°C cooling and 20% drying in the western hemisphere. The presence of the TP may have contributed greatly to the present milder climate in the NH. We are aware that our model results are subject to model limitation and may even be model dependent, since model bias exists in all complex models. In addition, the significance of our results needs to be verified by other coupled models. For that, we devote an appendix to discussion of the significance of our model results and our model bias.

This paper is organized as follows. An introduction to the model and experiments is given in [section 2](#). Atmosphere and ocean responses are analyzed in [sections 3](#) and [4](#), respectively. A summary and discussion are given in [section 5](#).

2. Model and experiments

The model used in this study is the Community Earth System Model (CESM) of the National Centre for Atmospheric Research (NCAR). It was also used in our previous studies (e.g., [Dai et al. 2017](#)). CESM is a fully coupled global climate model that provides state-of-the-art simulations of Earth's past, present, and future climate states (<http://www2.cesm.ucar.edu/>). CESM (version 1.0) consists of five components and one coupler: the Community Atmosphere Model (CAM5; [Park et al. 2014](#)), the Community Land Model (CLM4; [Lawrence et al. 2012](#)), the Community Ice Code (CICE4; [Hunke and Lipscomb 2010](#)), the Parallel Ocean Program (POP2; [Smith et al. 2010](#)), the Community Ice Sheet Model (Glimmer-CISM), and the CESM Coupler (CPL7). CESM1.0 has been widely used and validated by researchers in the community.

The model grid employed in this study is T31_gx3v7. The CAM5 has 26 vertical levels, with the finite volume nominal $3.75^\circ \times 3.75^\circ$ in the horizontal. It is essentially a new atmospheric model with more realistic formulations of radiation, boundary layer, and aerosols ([Meehl et al. 2013](#); [Neale et al. 2013](#)). The general features of the model formulation can be found in [Neale et al. \(2010\)](#) and [Park et al. \(2014\)](#). The CLM4 has the same horizontal resolution as CAM5. POP2 uses the grid gx3v7, which has 60 vertical levels, and a uniform 3.6° spacing in the zonal direction. In the meridional direction, the grid is nonuniformly spaced. It is 0.6° near the equator, gradually increasing to the maximum 3.4° at 35°N/S and then decreasing poleward. The model physics is described in details in [Danabasoglu et al. \(2012\)](#). CICE4 has the same horizontal grid as POP2. No flux adjustments are used in CESM1.0.

To explore the role of the TP in the formation of modern climate, two groups of topography experiments are carried out ([Fig. 1](#)). The first group includes a 2400-yr control run and a 400-yr experiment with the TP removed. The model geometry, topography, and continents of the control run are realistic ([Fig. 1a](#)), thus named "Real." The experiment without the TP, named "NoTibet," starts from year 2001 of Real, and is integrated for 400 years, with the topography around the TP set to 50 m above the sea level ([Fig. 1b](#)). The second group includes two experiments with modified topography, each starting from year 2001 of Real and is integrated for 400 years. One experiment has a global flat

topography that is 50 m above the sea level (named "Flat"; [Fig. 1c](#)). The other is similar to Flat, except the region of the TP has the realistic topography (named "OnlyTibet"; [Fig. 1d](#)). The changes in Earth's climate due to the TP removal are obtained by subtracting the results of Real from those of NoTibet. In comparison, the changes due to the presence of the TP are obtained by subtracting the results of Flat from those of OnlyTibet. By comparing these two groups of experiments, we can obtain a quantitative estimate of the TP's role in global climate with more confidence. Since Earth's climate changes in NoTibet (with respect to Real) are opposite to those in OnlyTibet (with respect to Flat), and they have roughly the same magnitude, we define the linear (or symmetric) and nonlinear (or asymmetric) changes due to the TP removal, respectively, as follows:

$$\begin{aligned} \text{Linear Change} \\ = [(\text{NoTibet} - \text{Real}) - (\text{OnlyTibet} - \text{Flat})]/2, \quad (1) \end{aligned}$$

$$\begin{aligned} \text{Nonlinear Change} \\ = [(\text{NoTibet} - \text{Real}) + (\text{OnlyTibet} - \text{Flat})]/2. \quad (2) \end{aligned}$$

In this work, we focus on the linear climate changes due to the TP removal. The nonlinear changes will not be discussed because they are very small in most regions. We will focus on the quasi-equilibrium (QE) responses of global climate, defined as the climate changes averaged over the last 100 years of the 400-yr integration; that is, only annual-mean climate changes are investigated. Note that the TP region specified in this work also includes the Mongolian Plateau (MP) ([Figs. 1b,d](#)). [Su et al. \(2018\)](#) have done a similar sensitivity experiment in which topography within the region of $20^\circ\text{--}60^\circ\text{N}$ and $60^\circ\text{--}140^\circ\text{E}$ at altitude higher than 200 m is set to 200 m, using the CESM version 1.0.5. This is slightly different from our experiments. Some studies found that the MP, despite its smaller size, exerts a great influence on the wintertime subtropical westerly jet ([Shi et al. 2015](#); [White et al. 2017](#)) and plays a significant role in strengthening the East Asian winter monsoon ([Sha et al. 2015](#)). For the summer monsoon circulation over the Euro-Asian region, these authors all stated that the TP plays a much more important role. In this work, we do not separate the roles of the TP and MP. A brief discussion on their relative roles will be given in [section 5](#).

3. Changes in global atmosphere

a. Energy balance at the top of atmosphere

[Figure 2](#) shows radiation fluxes at the top of atmosphere (TOA; positive value for downward flux). The

TP change causes a slight net energy imbalance in the Earth system, of about 0.1 PW (Fig. 2a, solid black curve) after 400-yr integration. Note that when the TP is removed, there is immediately a jump in both shortwave (SW) and longwave (LW) radiations at the TOA (Fig. 2a, blue and red curves), because of the immediate decrease in surface albedo and immediate surface warming due to lowered topography. Earth gains energy mainly via enhanced incoming SW radiation (solid blue curve), which is mostly balanced by enhanced outgoing LW radiation (solid red curve) during the first 200 years after the TP is removed. There are quick decreases in both SW and LW around year 200. The SW decrease is due to rapid southward expansion of sea ice from the Arctic Ocean (sea ice margin shown in Fig. 10b), while the LW decrease is due to strong cooling in the NH high latitudes. These changes are closely related to ocean dynamics, as discussed in Yang and Wen (2019). During the last 100 years of the 400-yr integration, the TOA energy imbalance is mainly due to the reduced outgoing LW, which in turn results from the global surface cooling (see section 3b and Fig. 6).

The changes in SW and LW at the TOA occur mainly in the NH around the latitudes of the TP region (Fig. 2b), and they are compensated with each other at most latitudes, leaving a small change in the net radiation flux. The QE changes in SW and LW are about 2.5% of their mean values, while the net radiation change is only 1% of its mean value. When the TP is removed, the enhanced SW near 30°N (Figs. 2b and 3b) is mainly due to reduced low clouds over the flattened TP region (Fig. 3e), which is consistent with reduced planetary albedo (Fig. 3d). The enhanced outgoing LW near 30°N (Figs. 2b and 3c) is mainly due to local surface warming caused by lowered topography and reduced high clouds (Fig. 3f) over the flattened TP region.

Figure 3 shows the horizontal patterns of TOA fluxes, albedo, and clouds. In the TP region, changes in radiative fluxes, albedo, and clouds are remarkable, as expected. When the TP is removed, both low and high clouds are reduced by about 30% (Figs. 3e,f), which are simply due to the anomalous high pressure caused by lowered topography. Because of the 4000-m height change, the anomalous high over the TP region is about 400 hPa (figure not shown), which greatly restrains the convection and moisture convergence, and thus the formation of clouds. Accordingly, the albedo is reduced by 20% (Fig. 3d), and both incoming SW and outgoing LW are enhanced (Figs. 3b,c). However, there are also two remote regions with notable changes in these radiation-related variables. One is over the North Atlantic, where the net incoming SW (Fig. 3b) and outgoing LW (Fig. 3c) are all reduced. The SW reduction is

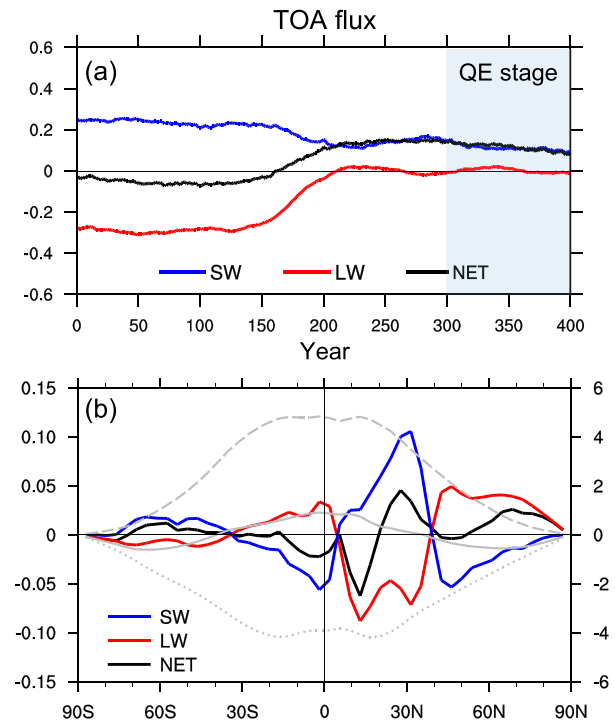


FIG. 2. Changes in radiation flux at the top of atmosphere (TOA) due to the TP removal. (a) Temporal evolutions of globally integrated net radiation flux (black), net downward shortwave (SW; blue), and net outgoing longwave (LW; red) at the TOA (PW; $1 \text{ PW} = 10^{15} \text{ W}$; positive for downward anomaly). The shaded rectangle shows the quasi-equilibrium (QE) stage of the experiments, which is used for making all time mean plots in this paper. (b) Time mean and zonally integrated radiative flux changes at the TOA (PW). Black, red, and blue curves are for the net flux, LW, and SW, respectively. Solid, dashed, and dotted gray curves are for the net radiative flux, net SW, and net LW fluxes in Real (scaled by the right y axis), respectively.

attributed to the increased low clouds and albedo over the midlatitudes and subpolar oceans (Figs. 3e,d). The LW gain is due to surface cooling (see discussion of Fig. 6), instead of high-cloud change (Fig. 3f). Another remote region with notable changes is the tropical Atlantic, where high clouds change the most. The high clouds (Fig. 3f) are reduced (increased) north (south) of the equator, suggesting a southward shift of deep convection over the tropical Atlantic, leading to a shift in the Atlantic intertropical convergence zone (ITCZ). This is also the consequence of cooling (warming) in the North (South) Atlantic caused by the weakening of the Atlantic meridional overturning circulation (AMOC). Accordingly, the outgoing LW (Fig. 3c) is enhanced (reduced) north (south) of the equator. The low clouds over the tropics are generally reduced (Fig. 3e). The change of clouds in the tropics does not affect albedo much (Fig. 3d), so the SW there does not change much (Fig. 3b).

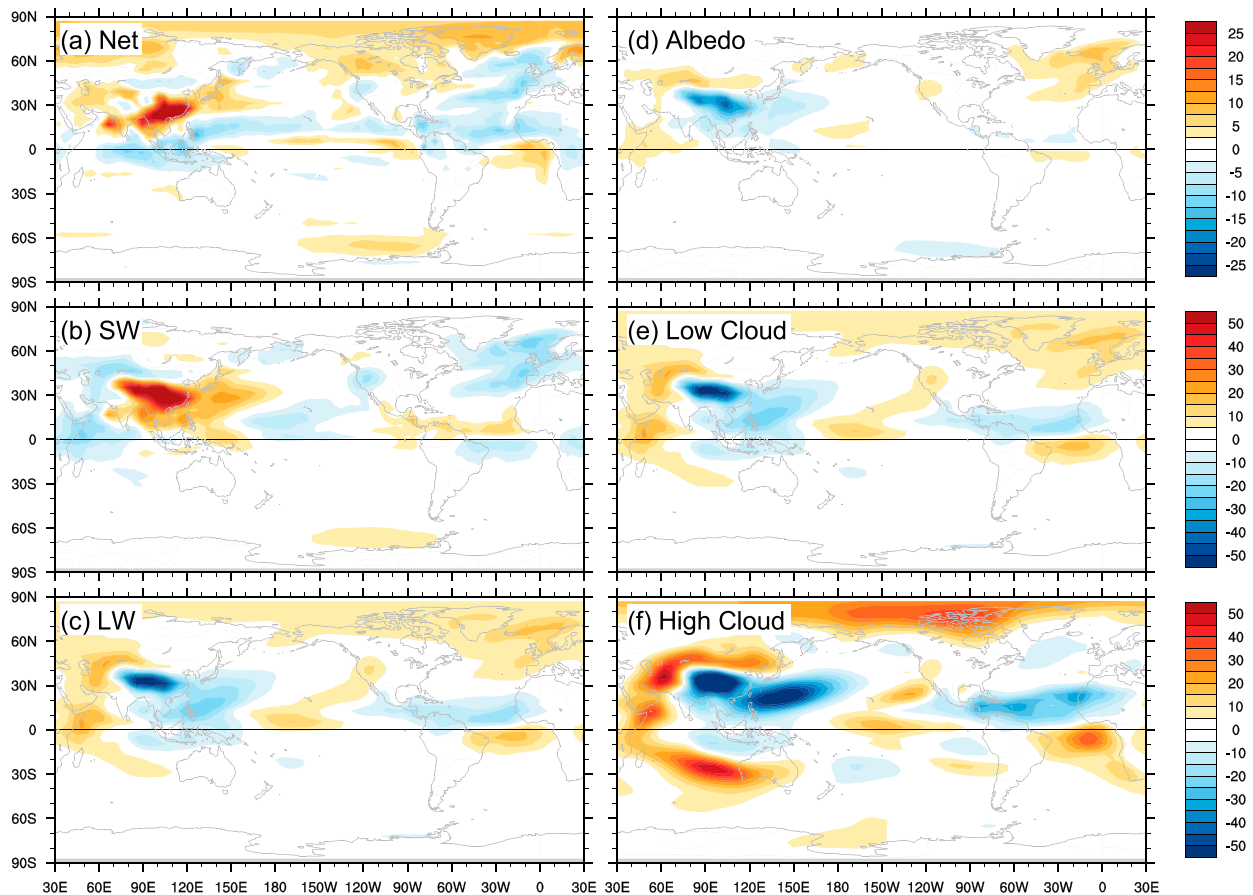


FIG. 3. QE changes in radiation flux and clouds due to the TP removal: (a) net radiative flux and (b) SW and (c) LW at the TOA. Units: W m^{-2} . Positive (negative) value represents downward (upward) flux. Also shown are (d)–(f) planetary albedo, low cloud, and high cloud, respectively. Units: percentage (%). Subplots in each row share the same color bar on the right.

b. Changes in global temperature and humidity

Without the TP, the NH would be 4°C cooler and the Southern Hemisphere (SH) would be 2°C warmer than the current reality (Fig. 4b). In other words, the presence of the TP alone could result in a maximum of about 4°C warming in the NH and 2°C cooling in the subpolar SH. Note that these temperature changes are not locally over the latitudes of the TP, but for the regions excluding the TP. Figure 4a shows the temporal evolution of surface temperature change averaged in the NH. For the surface air temperature (SAT), the local change over the TP region is excluded. First of all, it is straightforward that the SAT change is bigger than the sea surface temperature (SST) change due to the density difference between air and seawater. Second, in response to the TP removal, the NH is warming up in the first 100 years, and then cooling down quickly after 150 years. The QE response is that removing the TP will eventually result in significant surface cooling in the NH. The NH warming

in the beginning is caused by the strong local warming over the TP region due to the lowered topography (Fig. 6a) and is attributed to atmospheric dynamics only, whereas the warming reversal in the later stage is due to ocean dynamics, particularly thermohaline dynamics. We will show later that removing the TP would lead to more freshwater flux transport from the tropical Pacific to the North Atlantic, triggering a slowdown of the AMOC. The AMOC weakening will reduce the northward ocean heat transport and eventually cause remarkable cooling in the North Atlantic. The detailed processes involved are presented in Yang and Wen (2019). In a word, the slow evolution in the ocean thermohaline circulation leads to the surface temperature reversal in the NH.

The QE changes in zonal-mean SAT and SST are shown in Fig. 4b. The local SAT change over the TP region is again excluded. Qualitatively, it is well known that the TP has a strong influence on the NH climate. Here, we quantify it using our numerical experiments,

Corrigendum

The following figure is a corrigendum to Fig. 3e in our published paper “[Yang, H., X. Shen, J. Yao and Q. Wen, 2020: Portraying the impact of the Tibetan Plateau on global climate. *J. Climate*, 33\(9\), 3565-3583, doi: 10.1175/JCLI-D-18-0734.1](#)”. We are so sorry for the mistake due to our careless. This does not affect the analyses in the whole paper.

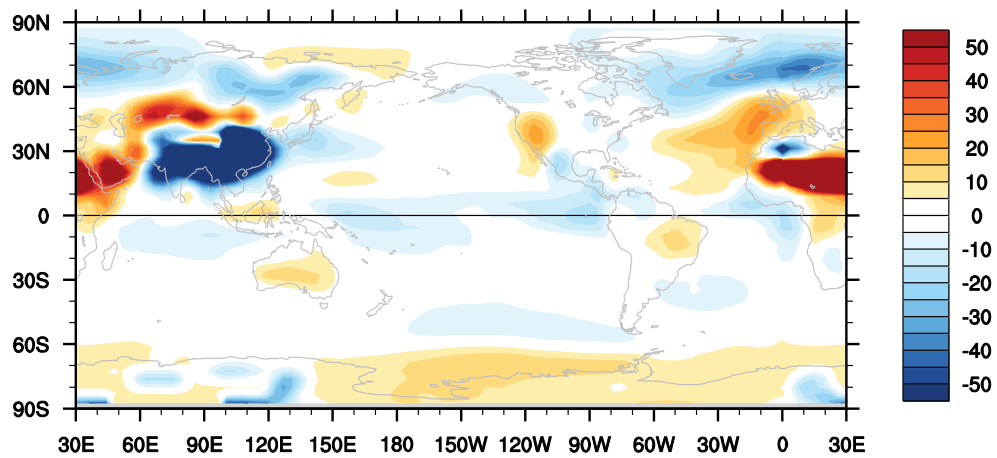


Figure 3e Quasi-equilibrium changes in low clouds due to the TP removal. Units: percentage (%).

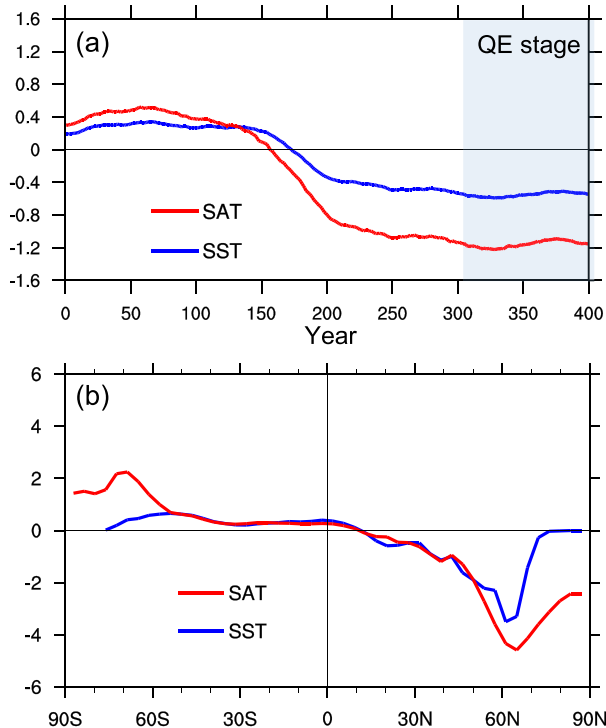


FIG. 4. Changes in SST and SAT due to the TP removal. (a) Temporal evolutions of SST changes (blue; $^{\circ}\text{C}$) and SAT changes (red; $^{\circ}\text{C}$) averaged over the NH, and (b) time and zonal mean changes in SAT (red) and SST (blue). Note that for SAT, the local change over the TP region is excluded.

namely, the absence (presence) of the TP can lead to as much as 4°C cooling (warming) in surface atmosphere, and about 3°C cooling (warming) in surface ocean (Fig. 4b). It is interesting to see that the absence (presence) of the TP alone can result in about 2°C warming (cooling) in the SH high latitudes (Fig. 4b). This strong remote effect of the TP on the SH needs careful investigation with more model experiments. Regardless, our experiments demonstrate that the presence of the TP plays an important role in the seesaw change between the two hemispheres, resulting in higher mean temperature in the NH than in the SH.

In fact, the entire air column would become colder without the TP. There is a cooling center in the upper level near 100 hPa over the NH polar region (Fig. 5b), which is even stronger than the surface cooling. The upper-level cooling center is separated from the surface cooling center, suggesting different mechanisms behind them. The surface cooling in the NH is almost totally attributed to ocean dynamics, that is, due to the weakening of the AMOC. This is further supported by our parallel slab-ocean experiments, in which no surface cooling occurred in the NH when the ocean dynamics was suppressed (figure not shown). The upper-level

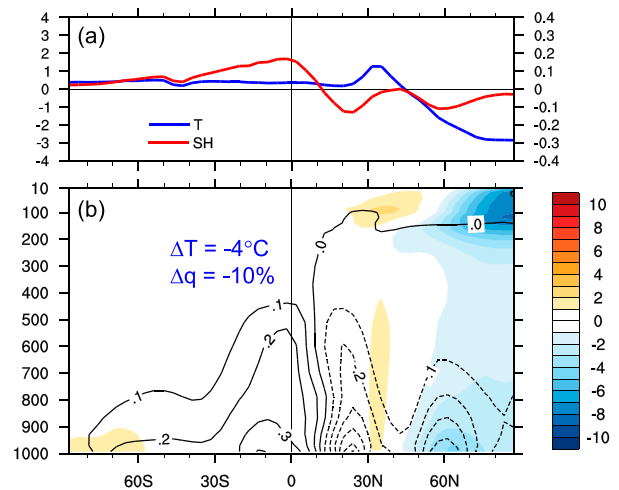


FIG. 5. Changes in atmospheric temperature and specific humidity due to the TP removal. (a) Temporally, zonally, and vertically averaged changes in air temperature (blue; $^{\circ}\text{C}$) and specific humidity (red; g kg^{-1}). (b) Zonal mean changes in air temperature (shading) and specific humidity (contour). The maximum changes in vertically averaged air temperature and specific humidity in the NH are given in (b).

cooling is a result of intensified polar vortex. Removing the TP intensifies the westerlies in the mid-to-high latitudes (see discussion of Fig. 7), weakens the poleward heat transport (see discussion of Fig. 12), and thus leads to a deepening of the polar vortex (Li 2015). In other words, the presence of the TP has resulted in the weakening of the westerlies in the NH, increasing the poleward atmosphere heat transport, and thus weakening the polar vortex. This will lead to remarkable warming in the upper-level atmosphere of the polar region. This situation was reported in White et al. (2018).

Without the TP, the NH would also become drier. The overall specific humidity, or the total precipitable water, in the NH atmosphere can be decreased by as much as 10%, accompanied by a 4°C cooling in the NH high latitudes (Fig. 5b). In other words, the presence of the TP can lead to 10% wetter NH, accompanied by a 4°C warming in the NH. It is straightforward that higher (lower) atmosphere temperature will cause more (less) evaporation from the surface, increasing (decreasing) the atmosphere moisture content (i.e., specific humidity). The TP plays an important role in regulating the moisture distribution between the two hemispheres. Apparently, the presence of the TP draws more moisture from the SH, carried by the northward cross-equatorial flow, which can increase the NH precipitation by as much as 10%. This is a tremendous contribution to the NH habitat.

Patterns of SAT and surface specific humidity reveal that the main changes actually occur in the western

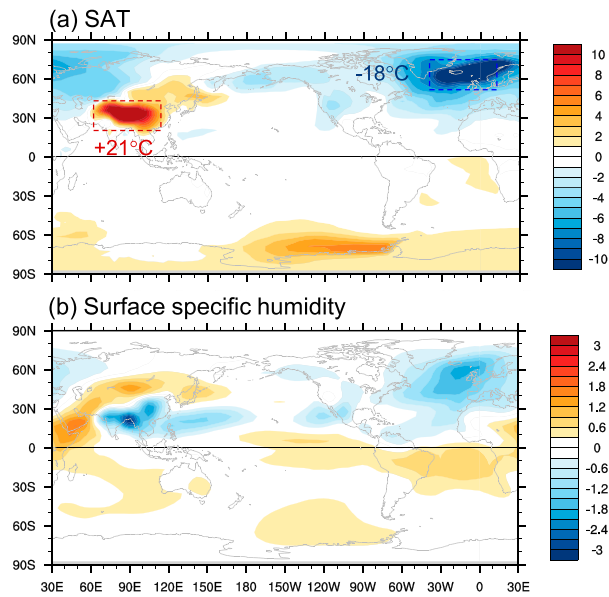


FIG. 6. QE changes in SAT and surface specific humidity due to the TP removal. (a) SAT ($^{\circ}\text{C}$) and (b) surface specific humidity (g kg^{-1}). The numbers in (a) indicate the maximum regional SAT changes.

hemisphere (Fig. 6). Without the TP, the cooling over the North Atlantic can be as much 18°C (Fig. 6a). Accordingly, the atmosphere there becomes much drier (Fig. 6b). In contrast to these remarkable changes over the North Atlantic, the changes elsewhere appear negligible. Figure 6 exhibits a strong remote effect of the TP on the North Atlantic. This teleconnection is established mainly via changes in atmosphere circulations, and will be discussed using Fig. 7 in section 3c. The strong cooling (warming) over the North Atlantic is determined by the AMOC change. It is the response of thermohaline circulation that ultimately controls the NH climate change. This also suggests a critical role of the TP in shaping the modern ocean circulations.

The local SAT response over the TP (Fig. 6a) is mainly due to the lowered topography. For an average height of 4000 m, the local SAT change would be about $24^{\circ}\text{--}28^{\circ}\text{C}$, given the lapse rate of wet air of $6^{\circ}\text{--}7^{\circ}\text{C km}^{-1}$. The actual local SAT increase is about 20°C , and 70%–80% of the lapse rate temperature change. Without the TP, surface specific humidity is reduced over the TP and increased around the northern rim of the TP (Fig. 6b). Note that the land surface specific humidity is not merely affected by local SAT. The precipitable water over the land is mainly determined by horizontal moisture transport, which is in turn determined by atmospheric circulation. This is remarkably different from that over the ocean. The atmospheric precipitable water over the ocean is mainly determined by local evaporation,

since the potential evaporation of the ocean is practically limitless as long as the air above is not saturated. Without the TP, the local surface specific humidity over the TP is reduced because of surface air divergence in response to the high pressure anomaly (due to lowered topography), while that around the northern rim of the TP is increased due to surface air convergence. This will be discussed further using Fig. 7 in section 3c.

Here, we briefly compare our results with those in previous studies. The pattern of SAT change in response to the TP removal (Fig. 6a) is consistent with that in previous studies (Kitoh 2002; Maffre et al. 2018). Different from previous studies, we emphasize in this work that the SAT change over the North Atlantic is mainly determined by ocean dynamics. It is straightforward that the change in orography will result in change in global precipitation pattern. For the local precipitation change, the implied precipitation change by surface specific humidity (Fig. 6b) around the TP and East Asia is consistent with the conclusions of Boos and Kuang (2013), Fallah et al. (2016), and Maffre et al. (2018). In particular, when the TP is removed, the moisture over the South China decreases, consistent with recent studies of Fallah et al. (2016) and Maffre et al. (2018). The moisture increase in the northern rim of the TP (Fig. 6b) is also consistent with early studies of Manabe and Broccoli (1990) and of Broccoli and Manabe (1992). For the implied remote precipitation change over the North Atlantic, we will show that it is mainly due to the moisture transport from the tropical Pacific along a so-called atmospheric river in the next subsection.

c. Changes in stationary waves and moisture transport

The dynamic effects of the TP on atmospheric circulations and moisture transport are shown in Fig. 7. The topography-forced stationary wave, along with the wave train, can be clearly seen in the pattern of sea level pressure (SLP) change (Fig. 7a). The structure of the wave train in the NH shows a northeastward propagation of wave energy (i.e., the group velocity), which establishes a robust teleconnection between the perturbation over the TP around 30°N and the atmosphere circulations over North America around $40^{\circ}\text{--}70^{\circ}\text{N}$ (Fig. 7a). The dynamics of TP-forced stationary wave can be well understood by the classic planetary wave theory in a linear quasigeostrophic system (Hoskins and Karoly 1981; Hoskins and Ambrizzi 1993). The energy propagation of the stationary wave can only occur within the westerlies in the mid-to-high latitudes, and the propagation direction is roughly determined by the ratio of meridional and zonal group velocities, which in turn is determined by the ratio of zonal and meridional scales

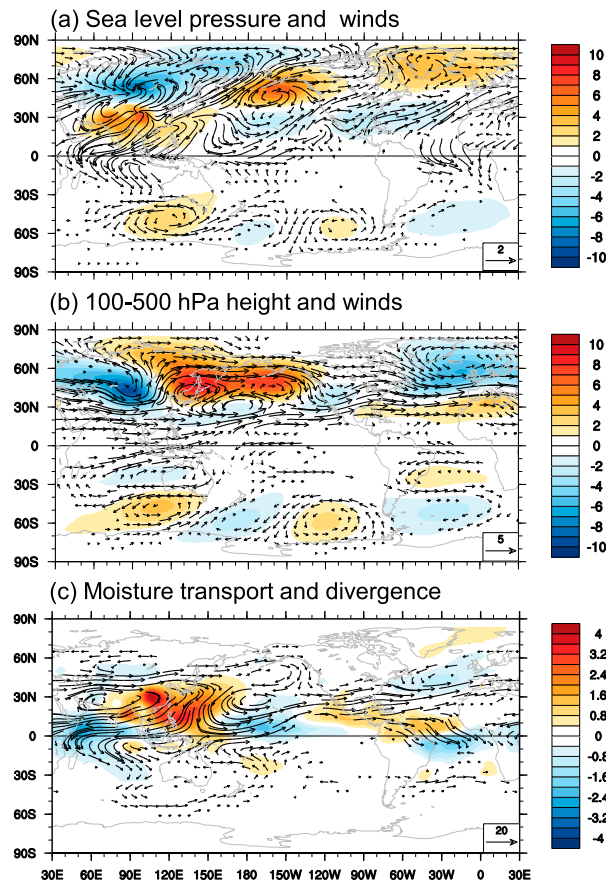


FIG. 7. QE changes in atmospheric pressure, wind, and moisture transport due to the TP removal. (a) SLP (shading; hPa) and wind (vector; m s^{-1}), (b) geopotential height (shading; 10 m) and wind averaged over 100–500 hPa, and (c) vertically integrated moisture transport ($\rho_a \mathbf{v}q$; $\text{kg m}^{-1} \text{s}^{-1}$) and its divergence [$\rho_a \nabla \cdot (\mathbf{v}q)$; shading; $10^{-5} \text{ kg m}^{-2} \text{ s}^{-1}$; positive for divergence and negative for convergence]. Atmosphere density $\rho_a = 1.29 \text{ kg m}^{-3}$.

of the perturbation (Pedlosky 1987). Mathematically, this can be formulated as $\tan\theta = (c_y/c_x) \sim (lk) \sim (L_x/L_y)$, where (c_x, c_y) , (k, l) , and (L_x, L_y) are zonal and meridional group velocities, wavenumbers, and horizontal scales of the perturbation, respectively. Given comparable L_x and L_y , the northeastward energy propagation of TP-excited stationary wave is manifested clearly (Fig. 7a), which leads to remarkable changes in the atmosphere circulations over the North Pacific and the subpolar Atlantic.

The TP-excited stationary wave train can be seen more clearly in the changes of geopotential height and wind in the upper-level atmosphere (Fig. 7b). These atmosphere changes have quasi-barotropic structures. We examine the vertically averaged changes over 100–500 hPa. When the TP is removed, an anomalous low develops north of the TP, along with a downstream

anomalous high over the subpolar Pacific and an anomalous low over the subpolar Atlantic (Fig. 7b), that is, an anomalous *low–high–low* pattern appears. Recall that the background structure of upper-level atmosphere in the mid-to-high latitudes is a zonal *high–low–high–low* pattern, that is, the Siberian high over the northeastern Eurasian continent, the Aleutian low over the subpolar Pacific, the North American high, and the Icelandic low over the subpolar Atlantic (figure not shown). The anomalous *low–high–low* pattern in the NH mid-to-high latitudes (Fig. 7b), that is, the stationary wave train, confirms the robust dynamic teleconnection between the atmosphere circulation over the TP and that over the North Atlantic, exhibiting an enhanced westerlies and a weakened meridional flow. In other words, the presence of the TP can result in weakened westerlies and enhanced meridional structure, contributing positively to the *high–low–high–low* pattern in the NH mid-to-high latitudes.

The teleconnection patterns shown in Fig. 7 agree well with those in previous studies (Zhao et al. 2007, 2009, 2011, 2012). The mechanism of teleconnection between the TP and atmosphere circulations over the North Pacific and North Atlantic has been studied using atmospheric general circulation models (AGCMs) (e.g., Zhao et al. 2007, 2009, 2012). The similar teleconnection patterns in our coupled climate model and in AGCMs (Zhao et al. 2007, 2009, 2012) suggest that this teleconnection is established mainly via atmospheric processes (Chiang and Bitz 2005; Broccoli et al. 2006; Zhao et al. 2012; Liu et al. 2013). We examined the atmospheric changes in the earlier stage of our model simulation (e.g., averaged over year 1 to year 50 of the model integration; figure not shown) and found them to be nearly identical to the QE changes shown in Fig. 7. This suggests that the ocean process does not feed back much to the teleconnection. In other words, the TP affects ocean circulation and buoyancy fields mainly via atmospheric processes (Fallah et al. 2016). This will be discussed further in section 4.

The atmospheric moisture transport is also modulated substantially by the TP. Without the TP, more freshwater would be transported from the tropical Pacific to the North Atlantic (Fig. 7c), which can weaken the North Atlantic Deep Water formation, triggering a weakening of the AMOC (Yang and Wen 2019). Since moisture transport ($\mathbf{v}q$) is determined by both atmospheric circulation (\mathbf{v}) and specific humidity (q), the $\mathbf{v}q$ pattern can be different from the circulation pattern. Figure 7c shows vertically integrated moisture transport and divergence ($\nabla \cdot \mathbf{v}q$) over the entire atmosphere column. It depicts the moisture transport pathway and the gain (or loss) of freshwater in both atmosphere and

ocean. Practically, in an equilibrium state the vertically integrated moisture divergence is equivalent to evaporation minus precipitation (EMP) over the ocean (Yang et al. 2015), when neglecting the freshwater flux of the land surface and river runoff and the change in atmospheric moisture content. Therefore, atmospheric moisture convergence ($\nabla \cdot \mathbf{v}q < 0$) represents a loss of atmosphere freshwater to the ocean ($\text{EMP} < 0$, or $E < P$), and vice versa. Without the TP, more atmosphere moisture will be transported all the way from the central tropical Pacific to the North Atlantic, converging over the North Atlantic (Fig. 7c), so that the atmosphere over the North Atlantic will become drier, while the North Atlantic Ocean will become fresher, which is consistent with reduced surface specific humidity (Fig. 6b). The atmosphere over the central tropical Pacific will also become drier. More importantly, without the TP the atmosphere over East Asia will become wetter ($\nabla \cdot \mathbf{v}q > 0$), suggesting more precipitable water over the land, which actually comes from the western tropical Pacific ($\text{EMP} > 0$); the atmosphere over the tropical Indian Ocean (20°S–20°N, 30°–100°E) will become drier ($\nabla \cdot \mathbf{v}q < 0$), because of a weakened (i.e., southward) cross-equatorial flow (Figs. 7a,c). In other words, our model experiments suggest that the presence of the TP can lead to a drier East Asia, a wetter tropical Indian Ocean, a fresher western Pacific, and a more saline North Atlantic, which are indeed consistent with the features of the present-day climate (Boos and Kuang 2010). These freshwater changes can be easily quantified using the outputs of the model experiments carried out in this work.

d. Hadley cell and Walker circulation

Because of its huge heating effect on the upper atmosphere in the boreal summertime (Wu et al. 2012a), the presence of the TP can shift the convective center over the Indian–Asian–Pacific (IAP) region toward the NH. Here, we estimate that removing the TP can result in more than 10% intensification of the northern branch of the Hadley cell (Fig. 8a), since the convective center over the IAP region shifts toward the equator, enhancing the deep convection over the western equatorial Pacific. This also leads to a more symmetric structure about the equator for the annual-mean Hadley cell. In other words, the presence of the TP contributes to the north–south asymmetry of the Hadley cell, and to the strong convection over the IAP region. We would like to emphasize that the intensity change of the Hadley cell is mostly due to the meridional displacement of the ascending branch of the cell, instead of intensified local ascending motion.

Without the TP, the Pacific Walker circulation in the tropics is weakened due to reduced convection over the

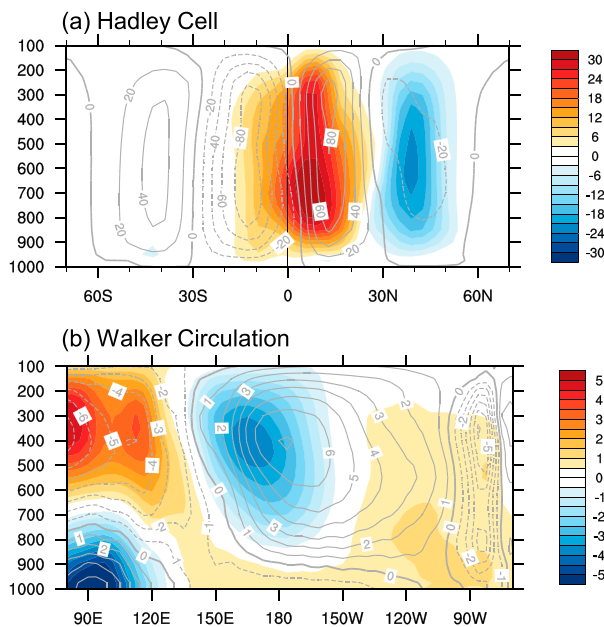


FIG. 8. QE changes in Hadley cell and Walker circulation due to the TP removal. (a) Hadley cell (shading; 10^9 kg s^{-1}) and (b) Walker circulation (shading; $10^{11} \text{ kg s}^{-1}$). Gray contours show the annual-mean Hadley cell and Walker circulation in Real. The maximum percentage changes in the Hadley cell and Walker circulation are about +15% at 10°N and –40% at 170°E, respectively.

western equatorial Pacific (Fig. 8b). This is accompanied by anomalous equatorial westerlies (Fig. 7a) and warmer SST (or a weakened cold tongue) in the eastern equatorial Pacific (see discussion of Fig. 10a), and thus a reduced downward motion over there. In other words, the presence of the TP contributes to the east–west asymmetry of the equatorial atmosphere convection by enhancing the upward motion over the Maritime Continent in the western equatorial Pacific and downward motion over the eastern equatorial Pacific, which is connected by stronger equatorial easterlies and thus forms a stronger cold tongue. The Walker circulation change in our experiments is similar to the finding by other studies using different coupled models (e.g., Naiman et al. 2017), implying a robust role of the TP in shaping the large-scale tropical atmosphere circulation.

4. Changes in the global ocean

Removing the TP in Asia can lead to strong surface cooling and freshening in the remote North Atlantic Ocean. In fact, we find as much as 8°C cooling and 4 psu freshening in the North Atlantic in our experiments. The surface freshening can eventually result in about 3 kg m^{-3} decrease in sea surface density, strong enough to shut down the AMOC.

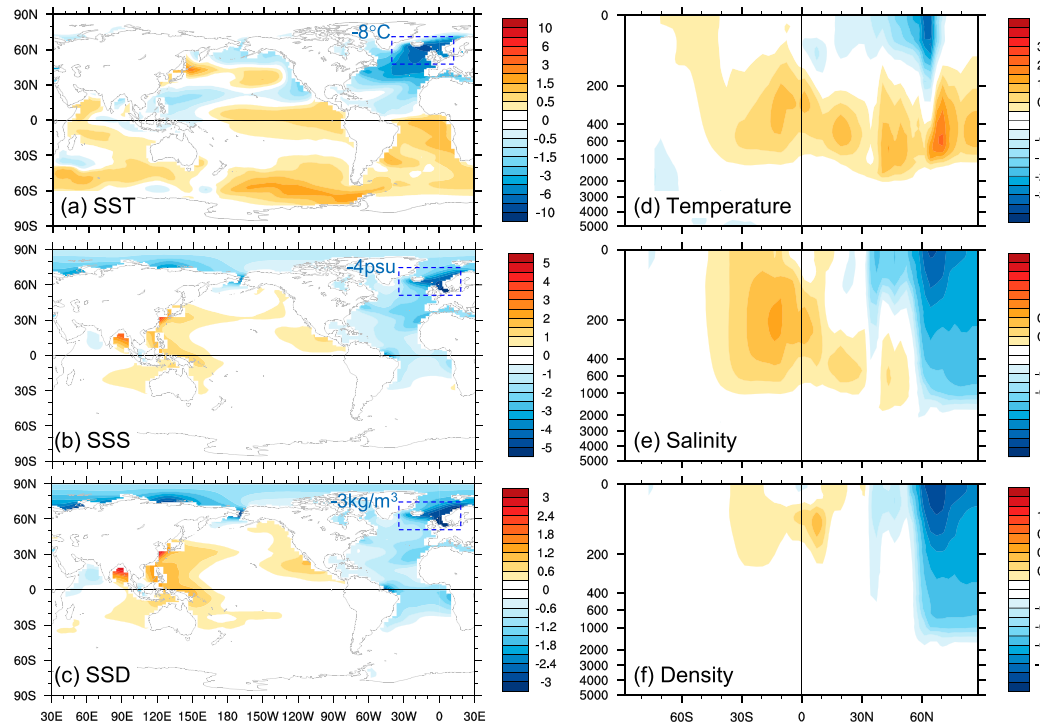


FIG. 9. QE changes in ocean buoyancy due to the TP removal: (a) SST ($^{\circ}\text{C}$), (b) sea surface salinity (SSS; psu), and (c) sea surface density (SSD; kg m^{-3}). The numbers show the maximum changes in SST, SSS, and SSD in the North Atlantic, respectively. (d)–(f) Zonally averaged global ocean temperature ($^{\circ}\text{C}$), salinity (psu), and density (kg m^{-3}), respectively.

a. Surface ocean buoyancy

Figure 9 shows QE changes in SST, sea surface salinity (SSS), and sea surface density (SSD). In response to the TP removal, there are strong remote cooling and freshening in the North Atlantic (Figs. 9a,b). Note that the SST and SSS changes in the Atlantic are qualitatively similar to the situation when adding freshwater to the North Atlantic (e.g., Manabe and Stouffer 1995; Zhang and Delworth 2005; Cheng et al. 2007; Yang et al. 2013); thus, the mechanisms for surface ocean changes are similar. Here, we briefly describe the critical processes. When the TP is removed, a large amount of atmospheric moisture is transported from the central tropical Pacific to the North Atlantic (Fig. 7c), resulting in a freshening of the North Atlantic surface ocean (Fig. 9b). This would reduce the deep-water formation in the Labrador Sea and Greenland–Iceland–Norwegian (GIN) Seas, triggering a slowdown of the AMOC. A chain reaction is thus set in motion. The AMOC slowdown results in less northward heat transport, cooling the North Atlantic. The sea ice in the subpolar region starts to expand southward (Fig. 10b), which brings more freshwater southward at the same

time. As the SSS decreases further, so does the deep-water formation in the North Atlantic. The surface freshening can be as much as 4 psu (Fig. 9b), which can decrease SSD by about 3 kg m^{-3} (Fig. 9c). The positive feedback between the southward expansion of sea ice and AMOC weakening can ultimately shut down the AMOC (Fig. 11a), which finally leads to as much as 8°C cooling in the North Atlantic (Fig. 9a).

The surface buoyancy change in response to the TP removal also exhibits interhemispheric and interbasin asymmetries. First, the shutdown of the AMOC can significantly reduce the northward ocean heat transport. Strong cooling occurs in the North Atlantic and several relatively weak warming regions occur in the South Atlantic (about 1.0°C), the eastern tropical Pacific (0.5°C), and the Southern Ocean (1.5°C) (Fig. 9a). The SST changes show more interhemispheric asymmetry. Second, due to anomalous eastward atmospheric moisture transport, strong freshening occurs in the North Atlantic, while weak salinization occurs in the western Pacific (1.0 psu) and the North Pacific (0.5 psu) (Fig. 9b). The SSS changes show more interbasin asymmetry. The SSS change appears to dominate the SSD change, and they have very similar spatial patterns (Figs. 9b,c). Here,

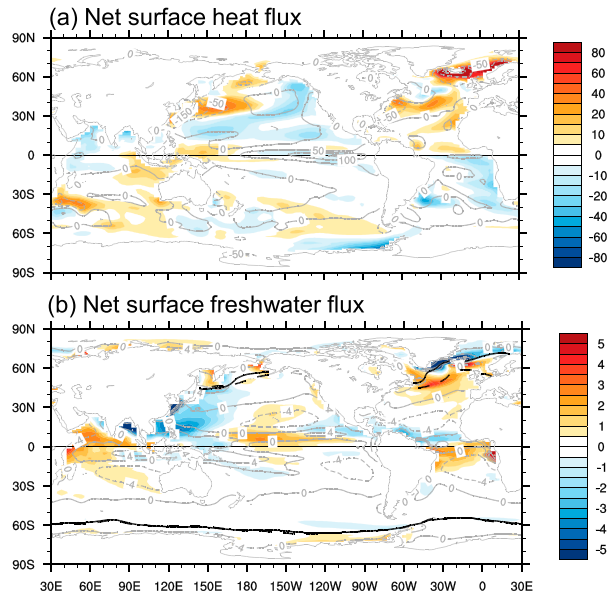


FIG. 10. QE changes in ocean surface flux due to the TP removal. (a) Net surface heat flux (shading; W m^{-2}), with positive (negative) for downward (upward) flux. (b) Net surface freshwater flux (shading; m s^{-1}), with positive (negative) for freshwater gain (loss) by the ocean. Gray contours in (a) and (b) show the annual-mean surface flux in Real. Solid and dashed curves in (b) show the sea ice margin in Real and NoTibet, respectively. The margin is defined as the 15% sea ice fraction in high-latitude oceans.

we want to emphasize that the SAT change over the North Atlantic (Fig. 6a) is actually forced by the SST change, on the time scale of interest in this work.

b. Surface heat flux and freshwater

To better understand the ocean change, we examine surface buoyancy flux change here. Figure 10 shows the QE changes in net surface heat flux and freshwater flux in response to the TP removal. Note that the net heat flux change can have either a damping effect or a driving effect on SST change, depending on which component dominates the net change, while the net surface freshwater flux change usually forces changes in SSS and SSD, which can be an important driving factor to the thermohaline circulation change.

To balance the strong surface cooling in the North Atlantic (Fig. 9a), the ocean gains heat at the surface by reducing both latent and sensible heat losses, and by reducing outgoing LW (Fig. 3c). On the contrary, to maintain the surface warming in the northwest Pacific, the ocean gains heat at the surface by enhancing incoming SW radiation (Fig. 3b), which is a result of decreased low cloud cover (Fig. 3e). The net surface heat flux plays a damping role in the North Atlantic cooling and a driving role in the northwest Pacific warming

(Fig. 10a). It also plays a damping role in the tropical and eastern Pacific warming. In the South Atlantic, the net surface heat flux is small but still has a damping effect on surface warming. The net surface heat flux plays a positive role in SST change mainly in the northwest Pacific, the South Pacific, and the southern Indian Ocean (Figs. 9a and 10a).

The horizontal pattern of surface freshwater flux (Fig. 10b) shows that the ocean gains freshwater in the Indian Ocean, the North Atlantic (including the Labrador Sea), the central tropical Pacific, and the southern equatorial Atlantic; and that the ocean loses freshwater in the western Pacific (including the South China Sea), the subpolar Atlantic (due to sea ice formation), and the northern equatorial Atlantic. The surface ocean freshwater gain (loss) is in good agreement with the atmospheric moisture convergence (divergence) over these regions (Fig. 7c), as discussed in section 3.

Sea ice melting (formation) also contributes to surface freshwater flux in the high latitudes (Fig. 10b). In fact, sea ice change in the subpolar North Atlantic dominates surface freshwater flux change there. The sea ice margin in the North Atlantic, denoted by the solid (for Real) and dashed (for NoTibet) black curves in Fig. 10b, shows a remarkable southward expansion in response to the TP removal. Sea ice formation occurs in the subpolar ocean, specifically in the GIN Seas, denoted by negative freshwater flux, which is the consequence of strong surface cooling in the North Atlantic (Fig. 9a). Sea ice melting occurs south of Iceland, accompanied by southward sea ice expansion, as denoted by the positive surface freshwater flux between the solid and dashed black curves (Fig. 10b). We want to emphasize that this sea ice melting is critical to the surface salinity decrease in the North Atlantic, and the weakening of the AMOC during years 150–200 after the TP removal, which causes a quick cooling in the NH (Fig. 4a). In fact, it is the positive feedback between sea ice melting and AMOC weakening that eventually shuts down the AMOC and causes the remarkable cooling in the North Atlantic. By modulating the atmospheric moisture transport (Fig. 7c), the surface freshwater flux change induced by the TP can trigger a change in the AMOC, which in turn initiates a meridional movement of sea ice in the subpolar ocean. Here, this TP effect on the NH sea ice is indirect. The direct impact of the TP on the Arctic sea ice is under investigation, and will be reported in future.

c. Upper-ocean changes

The surface buoyancy change can reach 2000 m (Figs. 9d–f). The ocean temperature response shows a baroclinic structure (Fig. 9d). A weakening of the AMOC

causes surface cooling in the North Atlantic, and at the same time a weakening of downward cold-water advection (i.e., a warming of subsurface water) (Fig. 9d). In other words, the surface cooling results in a shrinking of the surface water column and thus a stretching of subsurface water column (i.e., a warming of subsurface water). This kind of baroclinic response in the North Atlantic has been investigated comprehensively in model experiments (e.g., Manabe and Stouffer 1995; Zhang and Delworth 2005; Stouffer et al. 2007).

The ocean salinity response shows a barotropic structure (Fig. 9e). The surface ocean freshening in the North Atlantic is a combined result of sea ice melting and moisture transport from the tropical Pacific through the atmospheric bridge, as explained in section 3c. The subsurface freshening is mainly attributed to the weakened vertical saline water advection and diffusion. It is clear that the ocean density change is determined by salinity change; that is, a lower (higher) salinity results in a lighter (denser) water (Figs. 9e,f). This occurs not only in the North Atlantic but also in the tropical and southern oceans. This suggests once again that the hydrological cycle plays a critical role in ocean dynamics, and that the TP can modulate the global hydrological cycle to a great extent.

d. Meridional overturning circulations

The global ocean thermohaline circulations experience profound readjustment when the TP is removed. Specifically, the AMOC is nearly shut down (Fig. 11a) while a deep meridional overturning circulation develops in the Pacific (Fig. 11b) (i.e., Pacific meridional overturning circulation, or PMOC). In other words, the presence of the TP may provide a critical background in the formation of modern thermohaline circulation, that is, the deep and strong AMOC and the absence of a thermohaline circulation in the Pacific. By modulating the moisture transport between the Pacific and Atlantic, the TP can cause an interbasin seesaw of thermohaline circulations. In Fig. 11, the gray contours show the mean state of the overturning circulation, which includes both the upper-ocean wind-driven circulation and lower-ocean thermohaline circulation. The shading shows that the change of overturning circulation mainly occurs in the lower ocean (i.e., the thermohaline circulation).

It is interesting to see that the upper-ocean wind-driven circulation is only slightly affected when the TP is removed. The wind-driven circulation, say the subtropical cell (STC), has a symmetric structure about the equator (Schott et al. 2004). The surface poleward Ekman flow from the equator is balanced by the subsurface equatorward subsidence from the extratropics around 30°–40°N (°S), forming an anticyclonic (cyclonic)

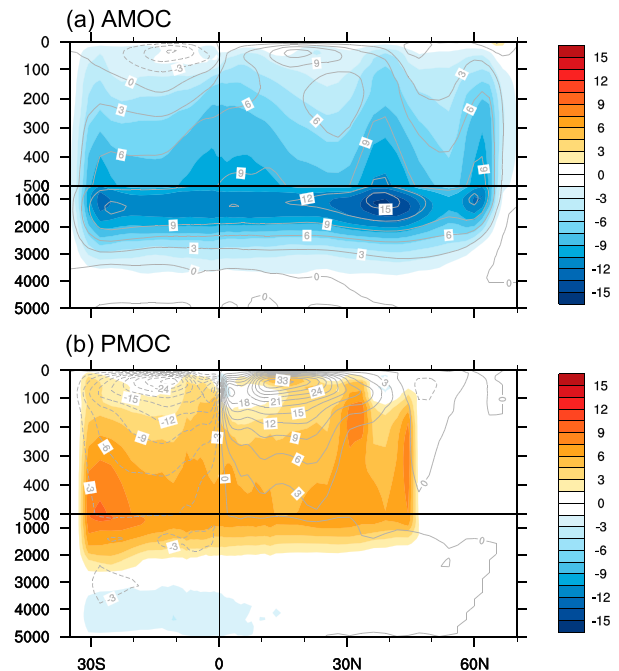


FIG. 11. QE changes in Atlantic meridional overturning circulation (AMOC) and Pacific meridional overturning circulation (PMOC) due to the TP removal: (a) AMOC (shading; Sv, 1 Sv = $10^6 \text{ m}^3 \text{ s}^{-1}$), and (b) PMOC (shading; Sv). Gray contours show the annual-mean AMOC and PMOC in Real.

shallow overturning circulation in the NH (SH). The STC is usually strong in the Pacific (Fig. 11b) and weaker in the Atlantic (Fig. 11a). The shading shows that the upper-ocean streamfunction only changes slightly. The northern (southern) branch of the Atlantic STC is weakened (enhanced) slightly (Fig. 11a). The opposite occurs in the Pacific; that is, the northern (southern) branch of Pacific STC is enhanced (weakened) slightly (Fig. 11b). In other words, the presence of the TP does not affect the formation of the wind-driven circulations in both the Pacific and Atlantic.

The changes in surface buoyancy and the AMOC presented here are consistent with Su et al. (2018), in which the same coupled model (but different version) was used and similar model experiments were performed. However, the physical explanation for these changes in our work is different from that given in Su et al. (2018). Detailed analyses can be found in Yang and Wen (2019). Su et al. (2018) did not show the initial warming of the NH and strengthening of the AMOC, and they believed that the northward moisture transport over the North Atlantic is critical to shut down the AMOC. Our study shows an initial strengthening, followed by a decline of the AMOC in response to the TP removal (Yang and Wen 2019). Moreover, we emphasize that the atmospheric moisture relocation from the tropical

Pacific to the North Atlantic is the key that triggers the weakening of the AMOC, and the positive feedback between the southward expansion of sea ice and AMOC leads to the AMOC shutdown. The differences in mechanisms suggest the complexity of the TP's role in affecting global ocean circulations. More sensitivity experiments using different models are needed to refine the mechanism at work.

e. Meridional heat transport and energy balance between two hemispheres

Earth's climate system is maintained by a hemispherically antisymmetric poleward heat transport with the peak value of about 5.5 PW (1 PW = 10^{15} W) at 40° N/S. The atmosphere heat transport (AHT) dominates poleward of $\sim 30^{\circ}$ N/S, while the ocean heat transport (OHT) dominates in the deep tropics (Fig. 12a). These features are well recognized in numerous studies (e.g., Held 2001; Trenberth and Caron 2001; Wunsch 2005; Czaja and Marshall 2006).

The northward OHT is weakened by as much as 0.4 PW (blue curve in Fig. 12b), about 20% of the peak OHT at 30° N, as a result of AMOC shutdown. The AHT is enhanced toward the north (red curve in Fig. 12b), due to the intensified Hadley cell, compensating the weakened OHT partly. Note that in the NH high latitudes, the northward AHT is also reduced, with the same sign as the OHT change. This is due to the weakened meridional wind in the mid-to-high latitudes, which reduces the northward dry-air static energy transport (solid black curve in Fig. 12c). It has been shown in Fig. 7b that without the TP, the westerlies in the midlatitudes are enhanced while the meridional wind is weakened. Note that the northward AHT in the mid-to-high latitudes due to eddy activities is enhanced (dashed curves in Fig. 12c). This may be attributed to the enhanced northward Rossby wave group velocity (Fig. 7a). In general, the weakened OHT and AHT in the midlatitudes contribute to the 4° C cooling in the extratropical NH (Fig. 4b). The weakened northward latent heat transport (solid blue curve in Fig. 12c) contributes to the dry climate in the NH. In other words, the presence of the TP results in a warmer and wetter NH, by enhancing both northward OHT and northward atmospheric moisture transport.

5. Summary and discussion

Through extreme topography experiments, we depicted global climate impact of the TP in this study. The presence of the TP alone may have resulted in about 4° C warmer and 10% wetter climate in the NH. We also quantify the remote effect of the TP on the Western

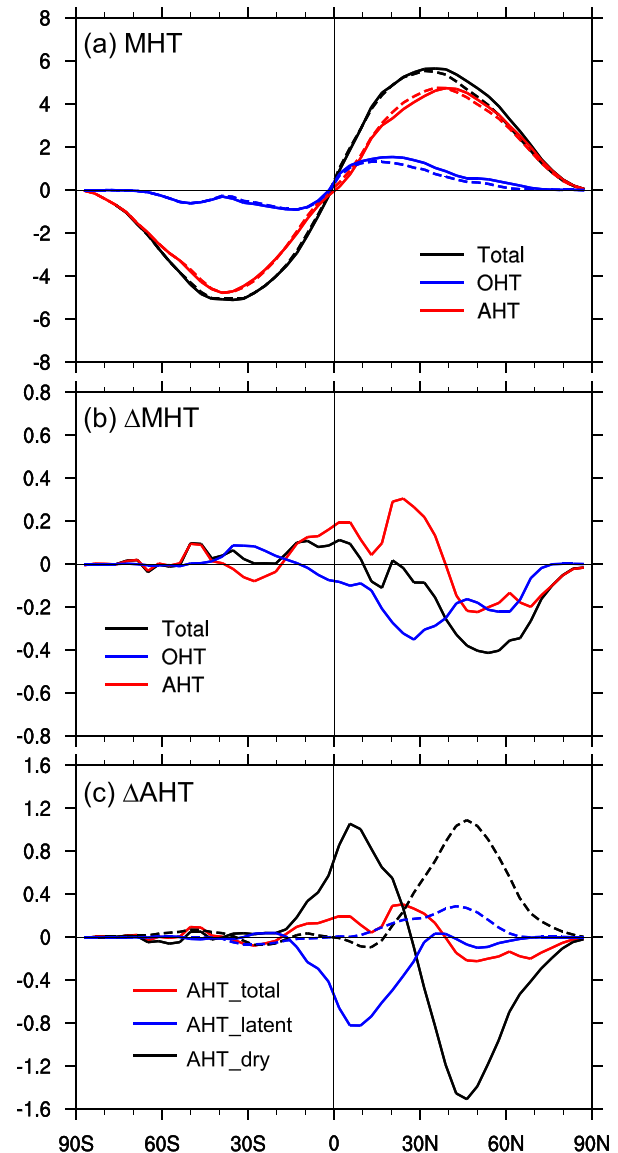


FIG. 12. Meridional heat transport (MHT) and its QE change due to the TP removal (units: PW). (a) Annual-mean MHT. Black, red, and blue curves represent the total MHT, atmosphere heat transport (AHT), and ocean heat transport (OHT), respectively. Solid and dashed curves are for Real and NoTibet, respectively. (b) Change in MHT. Black, red, and blue curves represent changes in total MHT, AHT, and OHT, respectively. (c) Change in the AHT component. Red curve is for the total AHT change, blue curve is for the latent heat component of AHT, and black curve is for the dry static energy of AHT. Solid and dashed curves represent those due to mean circulation and eddy activities, respectively.

Hemisphere, which is much stronger than on the Eastern Hemisphere. Without the TP, more freshwater would be transported from the central tropical Pacific to the North Atlantic, triggering the weakening of the AMOC, which can eventually result in more than 15° C

colder and 20% drier climate in the western hemisphere. Without the TP, the westerlies in the NH mid-to-high latitudes would be enhanced significantly, which would hinder the heat and moisture exchanges between the tropics and high latitudes, resulting in a much harsher climate in the NH high latitudes. Through its tremendous thermal and dynamic effects, the TP forces powerful stationary waves, which effectively convey local effects to remote regions, manifesting its great role in shaping the global climate.

This work focuses on the equilibrium changes of global climate in response to a sudden removal (adding) of the TP. From the perspective of paleoclimate studies, researchers pay more attention to the equilibrium response of Earth's climate to the movement of tectonic plates, due to its geological time scale. However, we must bear in mind that in response to the sudden TP change, the transient responses are dramatically different from the equilibrium responses. This can be seen in Fig. 4a, showing the global-mean surface temperature change from a warmer state in the transient stage to a much colder state in the equilibrium stage, after the TP is removed. We emphasize that this regime shift results from the change in global thermohaline circulation, which has a time scale of hundreds to thousands of years. One implication is that it is probably not suitable to study the past climate evolution using atmosphere-only models or coupled models with only slab ocean. Coupled models with full ocean dynamics are critical to obtain a reasonable understanding of Earth's climate evolution, because atmospheric temperature is ultimately determined by the ocean state. In addition, this work focuses on annual-mean climate changes. It is also important to explore seasonal climate changes forced by topography (Naiman et al. 2017; White et al. 2017), including the wintertime annular mode and westerlies, and the summertime Hadley cell and moisture transport. Detailed investigations of the transient changes and seasonal changes of the Earth climate in response to the TP change will be presented in a future paper.

Readers may notice that the topography change in our sensitivity experiments includes both the TP and the Mongolian Plateau (MP) (Fig. 1b). Some studies emphasized that despite its smaller size, the MP can also affect the winter atmospheric circulations over the Euro-Asian continent significantly. Shi et al. (2015) found that the MP can exert a great influence on the planetary-scale circulation and subtropical westerly jet. The authors used the model outputs from the experiments in Shi et al. (2015) and found that the MP plays a significant role in strengthening the East Asian winter monsoon. White et al. (2017) found that the MP and its nearby mountains have an impact on the upper-level

wintertime jet stream, which is much stronger than the impact by the TP and Himalayas to the south. All these studies emphasized that the MP effect is important for the *winter* atmospheric circulations. This is because during the wintertime, the East Asia monsoon blows southward and the impinging wind from the north is first affected by the MP (White et al. 2017). These studies also agreed that for the summer monsoon circulation, the TP plays a more important role. For example, Sha et al. (2015) showed that the Indian and East Asian summer monsoonal precipitation and inland precipitation are mainly enhanced by the uplift of the TP. Note that the conclusions of these studies were all based on the experiments from AGCMs. As we have mentioned earlier (see discussion of Fig. 4a), it is probably not suitable to study the past climate evolution using atmosphere-only models or coupled models with only slab ocean; coupled models with full ocean dynamics are necessary. In any case, we should identify the relative roles of the MP and TP in a coupled climate system in future work.

Although this is a highly idealized modeling study, it can help us understand the TP's role in the real world. For example, our model experiments suggest that there would be an enhanced meridional atmospheric heat and moisture transport across the equator over the Indian–western Pacific Ocean in the presence of the TP, which is consistent with that the rapid uplift of the TP during 10–8 Ma might have pushed the establishment of the monsoon system in East Asia (Kutzbach et al. 1993; An et al. 2001). Moreover, in the presence of the TP there would be more moisture transport from the North Atlantic to the tropical Pacific. This may increase the surface salinity and density in the North Atlantic, leading to strong deep-water formation over there. Since the timing of the rapid TP uplift is consistent with the timing (10 Ma) of the strong North Atlantic Deep Water formation (Ferreira et al. 2018, and references therein), our modeling results provide a mechanism to explain how the TP might have affected the formation of the AMOC.

It should be borne in mind that the conclusions drawn in this study are subject to model limitations, and may even be model-dependent. The potential impact of model bias, version, and resolution on the results may not be trivial. More details can be found in the appendix. In this work, we assume a stable model bias under different climate states with and without the TP, which may not be a valid assumption (Reifen and Toumi 2009; Kerkhoff et al. 2014). Model bias could distort the climate sensitivity to external forcing. Also, if ocean mixing or convection is not reasonably parameterized, the North Atlantic Deep Water formation may be more sensitive to surface buoyancy change than what happens

in the real world. This would exaggerate the AMOC change and thus the cooling of the NH. Model bias exists in complex models, and we should always be careful when interpreting model results.

Understanding the TP's role in global climate has profound significance. The significant warming over the TP region under the present climate background may cause subsequent global climate changes through possibly similar mechanisms to those presented in this paper, although the magnitude of current climate change is small compared to that caused by the removal of the TP. During the past half century, the TP showed a warming rate of $0.35^{\circ}\text{C decade}^{-1}$ (Xu et al. 2017), 3 times the warming rate of the global-mean surface temperature. Around the Lhasa region, the surface temperature increased even faster, at a rate of more than $0.5^{\circ}\text{C decade}^{-1}$ during 1963–2009 (Yin et al. 2013; Zhang et al. 2013; Kuang and Jiao 2016). There is an equivalent to 25 billion cubic meters of freshwater around the TP region (Yao et al. 2006). During the past century, more than 80% of the ice sheet around the TP has degenerated, and about 10% of the permafrost has been destroyed (Yao et al. 2006; Li et al. 2010). The melting of ice sheet and degeneration of permafrost have emerged as serious problems that we face today, and will have tremendous impact on the global environment. How much more will the TP be warmed? How will the future change around the TP feed back to the global warming? These imperative questions have drawn considerable attention from Chinese scientists, and the Third Tibetan Plateau Atmospheric Scientific Experiment (TIPEX-III) began formally in 2014 and will continue for 8–10 years to address these questions (Zhao et al. 2018). In-depth investigations on these questions will greatly enhance our ability to cope with the climate change in Asia and globally (Zhao et al. 2018, 2019). This work is only our first attempt to answer these questions, based on our model experiments. More investigations concerning the impact of future change around the TP on global climate, using different coupled models and through various sensitivity experiments, and combining with observations from the TIPEX-III, are urgently needed.

Acknowledgments. This work is supported by the NSF of China (Grants 91737204, 41725021, and 41376007). We greatly appreciate discussion with Prof. Z. Liu at Ohio State University, and invaluable suggestions from three anonymous reviewers. The experiments are performed on the supercomputers at the LaCOAS, Peking University, and the National Supercomputer Centre in Tianjin (Tian-He No.1).

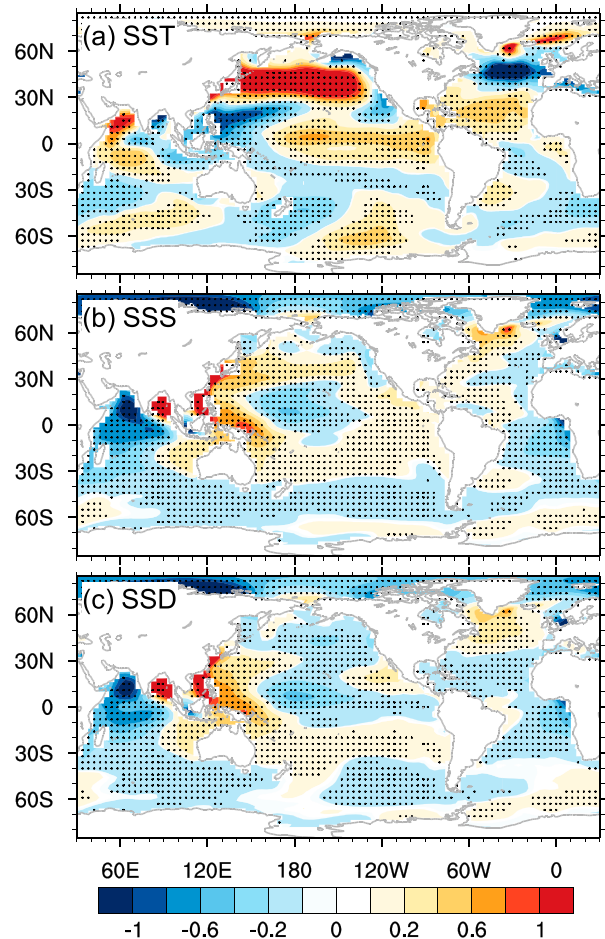


FIG. A1. Changes in (a) SST ($^{\circ}\text{C}$), (b) SSS (psu), and (c) SSD (kg m^{-3}) averaged over years 10–50 in NoTibet, with respect to Real. Stippling indicates changes exceeding the 95% significance level according to the Mann–Kendall trend test.

APPENDIX

Significance and Bias of Model Results

The changes of variables are significant in both transient stage and QE stage. In this work, we focus on the linear response of the global climate to the TP removal. These responses are mean state changes due to a strong external forcing (removing or adding the TP), and they usually have strong signals. This is not like “internal variability,” whose amplitude can be very small when compared to the mean state. We have performed the Mann–Kendall test for all figures related to changes, which are not shown in previous figures for cleanliness. Figure A1 shows the SST, SSS, and SSD changes in NoTibet with respect to Real. These changes are averaged over the transient stage of global climate (years 10–50).

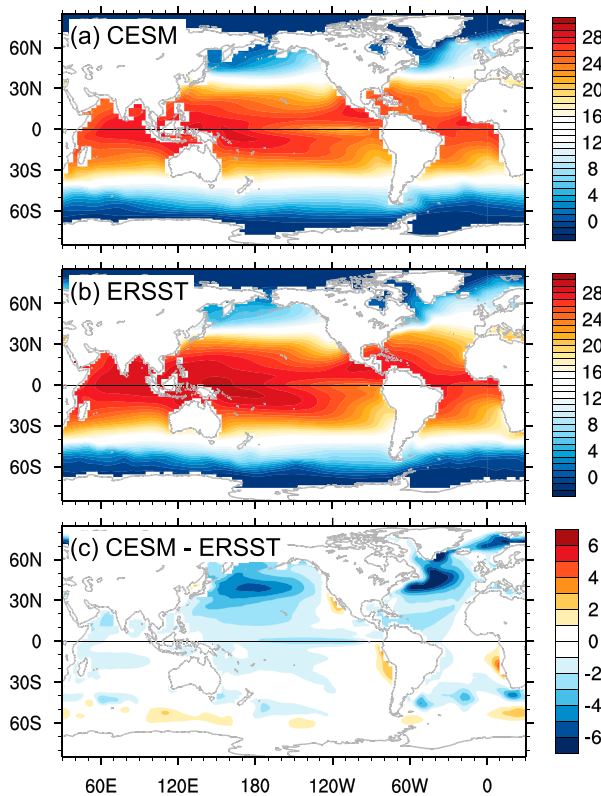


FIG. A2. Spatial patterns of mean SST ($^{\circ}\text{C}$) from (a) the CESM control run and (b) ERSST-v4 averaged between 1980 and 2018. After Huang et al. (2015). (c) SST bias of the CESM model, with respect to ERSST.

Stippling in Fig. A1 indicates that, according to the Mann–Kendall trend test, the changes of all these variables exceeding the 95% significance level in even the most remote regions in the Southern Ocean. The QE changes are much stronger than the transient changes, and are significant at the 99% level (figures not shown).

The impact of model bias and resolution on the results in this work is of another concern. The model bias of CESM with respect to the observations has been examined comprehensively in previous studies (<https://journals.ametsoc.org/topic/ccsm4-cesm1>). During this work, we also have examined model bias carefully. In general, the CESM can generally well simulate the mean climate observed.

First, we compared the meridional overturning circulation (MOC) in the Atlantic and Pacific from our CESM control simulation with that from ECCO-v4 ocean reanalysis (Forget et al. 2015). They are mostly consistent (figures not shown). For both sets of model outputs, the AMOC has a maximum value of about 15–20 Sv ($1 \text{ Sv} \equiv 10^6 \text{ m}^3 \text{ s}^{-1}$) at the depth range of 1000–1500 m, and the shallow wind-driven subtropical cell in

the Indo-Pacific basin has symmetric structure and a maximum value of more than 30 Sv at about 100 m. Second, the meridional heat transports calculated from CESM control simulation is in an excellent agreement with those based on observations (Trenberth and Caron 2001; Yang et al. 2015). Please also refer to Fig. 12a. Third, the mean SST pattern from CESM control simulation is generally in good agreement with that from ERSST-v4 (Huang et al. 2015) (Fig. A2). The SST bias in CESM is also clear. For example, the cold bias in the North Pacific and North Atlantic is significant (Fig. A2c), when compared with the observations (Fig. A2b). The lower SST in the North Atlantic may lead to a stronger AMOC than the reality. The warm pool in the western tropical Pacific is weaker than the observation, which may lead to a weaker Walker circulation in the tropics.

We also examined the mean climate of high-resolution model and that of low-resolution model, and found no significant differences between them, including the mean AMOC, the mean global SST and SAT, and the mean meridional heat transport [these are also examined in Yang et al. (2015)]. The sea ice cover in the low-resolution version is more extensive than that in the high-resolution version in the Pacific Ocean and Nordic seas. However, they are comparable in the subpolar North Atlantic and the Southern Ocean (figure not shown). The Labrador Sea is critical for deep-water formation and thermohaline circulation; fortunately, these are not affected much by model resolution.

REFERENCES

- An, Z., J. E. Kutzbach, W. L. Prell, and S. C. Porter, 2001: Evolution of Asian monsoons and phased uplift of the Himalaya–Tibetan plateau since Late Miocene times. *Nature*, **411**, 62–66, <https://doi.org/10.1038/35075035>.
- Boos, W. R., and Z. Kuang, 2010: Dominant control of the South Asian monsoon by orographic insulation versus plateau heating. *Nature*, **463**, 218–222, <https://doi.org/10.1038/nature08707>.
- , and —, 2013: Sensitivity of the South Asian monsoon to elevated and non-elevated heating. *Sci. Rep.*, **3**, 1192, <https://doi.org/10.1038/srep01192>.
- Broccoli, A. J., and S. Manabe, 1992: The effects of orography on midlatitude Northern Hemisphere dry climates. *J. Climate*, **5**, 1181–1201, [https://doi.org/10.1175/1520-0442\(1992\)005<1181:TEOOM>2.0.CO;2](https://doi.org/10.1175/1520-0442(1992)005<1181:TEOOM>2.0.CO;2).
- , K. A. Dahl, and R. J. Stouffer, 2006: Response of the ITCZ to Northern Hemisphere cooling. *Geophys. Res. Lett.*, **33**, L01702, <https://doi.org/10.1029/2005GL024546>.
- Cheng, W., C. M. Bitz, and J. C. H. Chang, 2007: Adjustment of the global climate to an abrupt slowdown of the Atlantic meridional overturning circulation. *Ocean Circulation: Mechanisms and Impacts—Past and Future Changes of Meridional Overturning*, *Geophys. Monogr.*, Vol. 173, Amer. Geophys. Union, 295–313.

- Chiang, J. C. H., and C. M. Bitz, 2005: Influence of high latitude ice cover on the marine Intertropical Convergence Zone. *Climate Dyn.*, **25**, 477–496, <https://doi.org/10.1007/s00382-005-0040-5>.
- Czaja, A., and J. Marshall, 2006: The partitioning of poleward heat transport between the atmosphere and ocean. *J. Atmos. Sci.*, **63**, 1498–1511, <https://doi.org/10.1175/JAS3695.1>.
- Dai, H., H. Yang, and J. Yin, 2017: Roles of energy conservation and climate feedback in Bjerknes compensation: A coupled modeling study. *Climate Dyn.*, **49**, 1513–1529, <https://doi.org/10.1007/S00382-016-3386-Y>.
- Danabasoglu, G., S. Bates, B. P. Briegleb, S. R. Jayne, M. Jochum, W. G. Large, S. Peacock, and S. G. Yeager, 2012: The CCSM4 ocean component. *J. Climate*, **25**, 1361–1389, <https://doi.org/10.1175/JCLI-D-11-00091.1>.
- Duan, A., and G. Wu, 2005: Role of the Tibetan Plateau thermal forcing in the summer climate patterns over subtropical Asia. *Climate Dyn.*, **24**, 793–807, <https://doi.org/10.1007/s00382-004-0488-8>.
- , and —, 2008: Weakening trend in the atmospheric heat source over the Tibetan Plateau during recent decades. Part I: Observations. *J. Climate*, **21**, 3149–3164, <https://doi.org/10.1175/2007JCLI1912.1>.
- Fallah, B., U. Cubasch, K. Prömmel, and S. Sodoudi, 2016: A numerical model study on the behaviour of Asian summer monsoon and AMOC due to orographic forcing of Tibetan Plateau. *Climate Dyn.*, **47**, 1485–1495, <https://doi.org/10.1007/s00382-015-2914-5>.
- Ferreira, D., and Coauthors, 2018: Atlantic–Pacific asymmetry in deep water formation. *Annu. Rev. Earth Planet. Sci.*, **46**, 327–352, <https://doi.org/10.1146/annurev-earth-082517-010045>.
- Forget, G., J. M. Campin, P. Heimbach, C. Hill, R. Ponte, and C. Wunsch, 2015: ECCO version 4: An integrated framework for non-linear inverse modeling and global ocean state estimation. *Geosci. Model Dev.*, **8**, 3071–3104, <https://doi.org/10.5194/gmd-8-3071-2015>.
- Gao, Y., H. Wang, and S. Li, 2013: Influences of the Atlantic Ocean on the summer precipitation of the southeastern Tibetan Plateau. *J. Geophys. Res. Atmos.*, **118**, 3534–3544, <https://doi.org/10.1002/JGRD.50290>.
- Harrison, T. M., P. Copeland, W. S. Kidd, and A. Yin, 1992: Raising Tibet. *Science*, **255**, 1663–1670, <https://doi.org/10.1126/science.255.5052.1663>.
- Held, I. M., 2001: The partitioning of the poleward energy transport between the tropical ocean and atmosphere. *J. Atmos. Sci.*, **58**, 943–948, [https://doi.org/10.1175/1520-0469\(2001\)058<0943:TPOTPE>2.0.CO;2](https://doi.org/10.1175/1520-0469(2001)058<0943:TPOTPE>2.0.CO;2).
- Hoskins, B. J., and D. J. Karoly, 1981: The steady linear response of a spherical atmosphere to thermal and orographic forcing. *J. Atmos. Sci.*, **38**, 1179–1196, [https://doi.org/10.1175/1520-0469\(1981\)038<1179:TSLROA>2.0.CO;2](https://doi.org/10.1175/1520-0469(1981)038<1179:TSLROA>2.0.CO;2).
- , and T. Ambrizzi, 1993: Rossby wave propagation on a realistic longitudinally varying flow. *J. Atmos. Sci.*, **50**, 1661–1671, [https://doi.org/10.1175/1520-0469\(1993\)050<1661:RWPOAR>2.0.CO;2](https://doi.org/10.1175/1520-0469(1993)050<1661:RWPOAR>2.0.CO;2).
- Huang, B., and Coauthors, 2015: Extended reconstructed sea surface temperature version 4 (ERSST.v4). Part I: Upgrades and intercomparisons. *J. Climate*, **28**, 911–930, <https://doi.org/10.1175/JCLI-D-14-00006.1>.
- Hunke, E. C., and W. H. Lipscomb, 2010: CICE: The Los Alamos Sea Ice Model, documentation and software user’s manual, version 4.1. Version 4.0, LA-CC-06-012, Los Alamos National Laboratory, 76 pp.
- Kerckhoff, C., H. R. Künsch, and C. Schär, 2014: Assessment of bias assumptions for climate models. *J. Climate*, **27**, 6799–6818, <https://doi.org/10.1175/JCLI-D-13-00716.1>.
- Kitoh, A., 2002: Effects of large-scale mountains on surface climate: A coupled ocean–atmosphere general circulation model study. *J. Meteor. Soc. Japan*, **80**, 1165–1181, <https://doi.org/10.2151/jmsj.80.1165>.
- Kuang, X., and J. J. Jiao, 2016: Review on climate change on the Tibetan Plateau during the last half century. *J. Geophys. Res.*, **121**, 3979–4007, <https://doi.org/10.1002/2015JD024728>.
- Kutzbach, J. E., P. J. Guetter, W. F. Ruddiman, and W. L. Prell, 1989: Sensitivity of climate to late Cenozoic uplift in southern Asia and the American west: Numerical experiments. *J. Geophys. Res.*, **94**, 18 393–18 407, <https://doi.org/10.1029/JD094iD15p18393>.
- , —, P. J. Behling, and R. Selin, 1993: Simulated climatic changes: Results of the COHMAP climate-model experiments. *Global Climates Since the Last Glacial Maximum*. H. E. Wright et al., Eds., University of Minnesota Press, 24–93.
- Lawrence, D. M., K. W. Oleson, M. G. Flanner, C. G. Fletcher, P. J. Lawrence, S. Levis, S. C. Swenson, and G. B. Bonan, 2012: The CCSM4 land simulation, 1850–2005: Assessment of surface climate and new capabilities. *J. Climate*, **25**, 2240–2260, <https://doi.org/10.1175/JCLI-D-11-00103.1>.
- Li, L., S. Yang, Z. Wang, X. Zhu, and H. Tang, 2010: Evidence of warming and wetting climate over the Qinghai-Tibet Plateau. *Arct. Antarct. Alp. Res.*, **42**, 449–457, <https://doi.org/10.1657/1938-4246-42.4.449>.
- Li, X., 2015: Review of the introduction and debates of the annular modes. *Adv. Earth Sci.*, **30**, 367–384.
- Liu, Y., G. M. Henderson, C. Hu, A. J. Mason, N. Charnley, K. R. Johnson, and S. Xie, 2013: Links between the East Asian monsoon and North Atlantic climate during the 8,200 year event. *Nat. Geosci.*, **6**, 117–120, <https://doi.org/10.1038/ngeo1708>.
- Maffre, P., J. B. Ladant, Y. Donnadieu, P. Sepulchre, and Y. Goddérís, 2018: The influence of orography on modern ocean circulation. *Climate Dyn.*, **50**, 1277–1289, <https://doi.org/10.1007/s00382-017-3683-0>.
- Manabe, S., and A. J. Broccoli, 1990: Mountains and arid climates of middle latitudes. *Science*, **247**, 192–195, <https://doi.org/10.1126/science.247.4939.192>.
- , and R. J. Stouffer, 1995: Simulation of abrupt climate change induced by freshwater input to the North Atlantic Ocean. *Nature*, **378**, 165–167, <https://doi.org/10.1038/378165a0>.
- Meehl, G. A., 1994: Coupled land–ocean–atmosphere processes and South Asian monsoon variability. *Science*, **266**, 263–267, <https://doi.org/10.1126/science.266.5183.263>.
- , and Coauthors, 2013: Climate change projections in CESM1 (CAM5) compared to CCSM4. 672. *J. Climate*, **26**, 6287–6308, <https://doi.org/10.1175/JCLI-D-12-00572.1>.
- Molnar, P., P. England, and J. Martinod, 1993: Mantle dynamics, uplift of the Tibetan Plateau, and the Indian monsoon. *Rev. Geophys.*, **31**, 357–396, <https://doi.org/10.1029/93RG02030>.
- Naiman, Z., P. Goodman, J. P. Krasting, S. L. Malyshev, J. L. Russell, R. J. Stouffer, and A. T. Wittenberg, 2017: Impact of mountains on tropical circulation in two Earth system models. *J. Climate*, **30**, 4149–4163, <https://doi.org/10.1175/JCLI-D-16-0512.1>.
- Neale, R. B., and Coauthors, 2010: Description of the NCAR Community Atmosphere Model (CAM5.0). NCAR Tech. Rep. NCAR/TN-486+STR, National Center for Atmospheric Research, 268 pp., www.cesm.ucar.edu/models/cesm1.1/cam/docs/description/cam5_desc.pdf.

- , J. Richter, S. Park, P. Lauritzen, S. Vavrus, P. Rasch, and M. Zhang, 2013: The mean climate of the Community Atmosphere Model (CAM4) in forced SST and fully coupled experiments. *J. Climate*, **26**, 5150–5168, <https://doi.org/10.1175/JCLI-D-12-00236.1>.
- Park, S., C. S. Bretherton, and P. J. Rasch, 2014: Integrating cloud processes in the Community Atmosphere Model, version 5. *J. Climate*, **27**, 6821–6856, <https://doi.org/10.1175/JCLI-D-14-00087.1>.
- Pedlosky, J., 1987: *Geophysical Fluid Dynamics*. 2nd ed. Springer-Verlag, 710 pp., <https://doi.org/10.1007/978-1-4612-4650-3>.
- Rea, D. K., H. Snoeckx, and L. H. Joseph, 1998: Late Cenozoic eolian deposition in the North Pacific: Asian drying, Tibetan uplift, and cooling of the Northern Hemisphere. *Paleoceanography*, **13**, 215–224, <https://doi.org/10.1029/98PA00123>.
- Reifen, C., and R. Toumi, 2009: Climate projections: Past performance no guarantee of future skill? *Geophys. Res. Lett.*, **36**, L13704, <https://doi.org/10.1029/2009GL038082>.
- Ruddiman, W. F., and J. E. Kutzbach, 1989: Forcing of Late Cenozoic Northern Hemisphere climate by plateau uplift in southern Asia and the American West. *J. Geophys. Res.*, **94**, 18 409–18 427, <https://doi.org/10.1029/JD094iD15p18409>.
- Schmittner, A., T. A. M. Silva, K. Fraedrich, E. Kirk, and F. Lunkeit, 2011: Effects of mountains and ice sheets on global ocean circulation. *J. Climate*, **24**, 2814–2829, <https://doi.org/10.1175/2010JCLI3982.1>.
- Schott, F. A., J. P. McCreary, and G. C. Johnson, 2004: Shallow overturning circulations of the tropical–subtropical oceans. *Earth's Climate: The Ocean-Atmosphere Interaction*, Geophys. Monogr., Vol. 147, Amer. Geophys. Union, 261–304, <https://doi.org/10.1029/147GM15>.
- Sha, Y., Z. Shi, X. Liu, and Z. An, 2015: Distinct impacts of the Mongolian and Tibetan Plateaus on the evolution of the East Asian monsoon. *J. Geophys. Res.*, **120**, 4764–4782, <https://doi.org/10.1002/2014JD022880>.
- Shi, Z., X. Liu, Y. Liu, Y. Sha, and T. Xu, 2015: Impact of Mongolian Plateau versus Tibetan Plateau on the westerly jet over North Pacific Ocean. *Climate Dyn.*, **44**, 3067–3076, <https://doi.org/10.1007/s00382-014-2217-2>.
- Sinha, B., A. T. Blaker, J. J.-M. Hirschi, S. Bonham, M. Brand, S. Josey, R. S. Smith, and J. Marotzke, 2012: Mountain ranges favour vigorous Atlantic meridional overturning. *Geophys. Res. Lett.*, **39**, L02705, <https://doi.org/10.1029/2011GL050485>.
- Smith, R. D., and Coauthors, 2010: The Parallel Ocean Program (POP) reference manual. Tech. Rep. LAUR-10-01853, Los Alamos National Laboratory, 140 pp.
- Stouffer, R. J., D. Seidov, and B. J. Haupt, 2007: Climate response to external sources of freshwater: North Atlantic versus the Southern Ocean. *J. Climate*, **20**, 436–448, <https://doi.org/10.1175/JCLI4015.1>.
- Su, B., D. Jiang, R. Zhang, P. Sepulchre, and G. Ramstein, 2018: Difference between the North Atlantic and Pacific meridional overturning circulation in response to the uplift of the Tibetan Plateau. *Climate Past*, **14**, 751–762, <https://doi.org/10.5194/cp-14-751-2018>.
- Trenberth, K. E., and J. M. Caron, 2001: Estimates of meridional atmosphere and ocean heat transports. *J. Climate*, **14**, 3433–3443, [https://doi.org/10.1175/1520-0442\(2001\)014<3433:EOMAAO>2.0.CO;2](https://doi.org/10.1175/1520-0442(2001)014<3433:EOMAAO>2.0.CO;2).
- Wang, Y., and Coauthors, 2005: The Holocene Asian monsoon: Links to solar changes and North Atlantic climate. *Science*, **308**, 854–857, <https://doi.org/10.1126/science.1106296>.
- White, R. H., D. S. Battisti, and G. H. Roe, 2017: Mongolian mountains matter most: Impacts of the latitude and height of Asian orography on Pacific wintertime atmosphere circulation. *J. Climate*, **30**, 4065–4082, <https://doi.org/10.1175/JCLI-D-16-0401.1>.
- , —, and A. Sheshadri, 2018: Orography and boreal winter stratosphere: The importance of the Mongolian mountains. *Geophys. Res. Lett.*, **45**, 2088–2096, <https://doi.org/10.1002/2018GL077098>.
- Wu, G., 2004: Recent progress in the study of the Qinghai-Xizang Plateau climate dynamics in China. *Quat. Sci.*, **24**, 1–9.
- , and Coauthors, 1997: Sensible heat driven air-pump over the Tibetan Plateau and its impacts on the Asian summer monsoon (in Chinese). *Collections in Memory of Zhao Jiuzhang*, D.-Z. Ye, Ed., Science Press, 116–126.
- , J. Wang, and X. Liu, 2005: Numerical modeling of the influence of Eurasian orography on the atmospheric circulation in different seasons (in Chinese). *Acta Meteor. Sin.*, **63**, 603–612.
- , Y. Liu, Q. Zhang, and A. Duan, 2007: The influence of mechanical and thermal forcing by the Tibetan Plateau on Asian climate. *J. Hydrometeorol.*, **8**, 770–789, <https://doi.org/10.1175/JHM609.1>.
- , —, B. He, Q. Bao, A. Duan, and F.-F. Jin, 2012a: Thermal controls on the Asian summer monsoon. *Sci. Rep.*, **2**, 404, <https://doi.org/10.1038/srep00404>.
- , —, B. Dong, X. Liang, A. Duan, Q. Bao, and J. Yu, 2012b: Revisiting Asian monsoon formation and change associated with Tibetan Plateau forcing: I. Formation. *Climate Dyn.*, **39**, 1169–1181, <https://doi.org/10.1007/S00382-012-1334-Z>.
- , and Coauthors, 2015: Tibetan Plateau climate dynamics: Recent progress and outlook. *Natl. Sci. Rev.*, **2**, 100–116, <https://doi.org/10.1093/nsr/nwu045>.
- Wunsch, C., 2005: The total meridional heat flux and its oceanic and atmospheric partition. *J. Climate*, **18**, 4374–4380, <https://doi.org/10.1175/JCLI3539.1>.
- Xu, Y., A. Knudby, H. C. Ho, Y. Shen, and Y. Liu, 2017: Warming over the Tibetan Plateau in the last 55 years based on area-weighted average temperature. *Reg. Environ. Change*, **17**, 2339–2347, <https://doi.org/10.1007/s10113-017-1163-z>.
- Yanai, M. H., C. F. Li, and Z. Song, 1992: Seasonal heating of the Tibetan Plateau and its effects of the evolution of the Asian summer monsoon (in Japanese). *J. Meteor. Soc. Japan*, **70**, 319–351, https://doi.org/10.2151/jmsj1965.70.1B_319.
- Yang, H., and Q. Wen, 2019: Investigating the role of the Tibetan Plateau in the formation of Atlantic meridional overturning circulation. *J. Climate*, **33**, 3585–3601, <https://doi.org/10.1175/JCLI-D-19-0205.1>.
- , Y. Wang, and Z. Liu, 2013: A modelling study of the Bjerknes compensation in the meridional heat transport in a freshening ocean. *Tellus*, **65A**, 18480, <https://doi.org/10.3402/tellusa.v65i0.18480>.
- , Q. Li, K. Wang, Y. Sun, and D. Sun, 2015: Decomposing the meridional heat transport in the climate system. *Climate Dyn.*, **44**, 2751–2768, <https://doi.org/10.1007/s00382-014-2380-5>.
- Yao, T. D., Z. Li, L. G. Thompson, E. Mosley-Thompson, Y. Wang, L. Tian, N. Wang, and K. Duan, 2006: $\delta^{18}\text{O}$ records from Tibetan ice cores reveal differences in climatic changes. *Ann. Glaciol.*, **43**, 1–7, <https://doi.org/10.3189/172756406781812131>.
- , and Coauthors, 2012: Different glacier status with atmospheric circulations in Tibetan Plateau and surroundings. *Nat. Climate Change*, **2**, 663–667, <https://doi.org/10.1038/nclimate1580>.

- Yeh, T. C., and Y. Gao, 1979: *Meteorology of the Qinghai-Xizang Plateau* (in Chinese). Science Press, 328 pp.
- , S. Lo, and P. Chu, 1957: The wind structure and heat balance in the lower troposphere over Tibetan Plateau and its surroundings (in Chinese). *Acta Meteor. Sin.*, **28**, 108–121.
- Yin, Y., S. Wu, D. Zhao, D. Zheng, and T. Pan, 2013: Modeled effects of climate change on actual evapotranspiration in different eco-geographical regions in the Tibetan Plateau. *J. Geogr. Sci.*, **23**, 195–207, <https://doi.org/10.1007/s11442-013-1003-0>.
- Zhang, D., J. Huang, X. Guan, B. Chen, and L. Zhang, 2013: Long-term trends of precipitable water and precipitation over the Tibetan Plateau derived from satellite and surface measurements. *J. Quant. Spectrosc. Radiat. Transfer*, **122**, 64–71, <https://doi.org/10.1016/j.jqsrt.2012.11.028>.
- Zhang, R., and T. L. Delworth, 2005: Simulated tropical response to a substantial weakening of the Atlantic thermohaline circulation. *J. Climate*, **18**, 1853–1860, <https://doi.org/10.1175/JCLI3460.1>.
- Zhao, P., Y. Zhu, and R. Zhang, 2007: An Asian–Pacific teleconnection in summer tropospheric temperature and associated Asian climate variability. *Climate Dyn.*, **29**, 293–303, <https://doi.org/10.1007/s00382-007-0236-y>.
- , X. Zhang, Y. Li, and J. Chen, 2009: Remotely modulated tropical–North Pacific ocean–atmosphere interactions by the South Asian high. *Atmos. Res.*, **94**, 45–60, <https://doi.org/10.1016/j.atmosres.2009.01.018>.
- , S. Yang, M. Jian, and J. Chen, 2011: Relative controls of Asian–Pacific summer climate by Asian land and tropical–North Pacific sea surface temperature. *J. Climate*, **24**, 4165–4188, <https://doi.org/10.1175/2011JCLI3915.1>.
- , —, R. Wu, Z. Wen, J. Chen, and H. Wang, 2012: Asian origin of interannual variations of summer climate over the extratropical North Atlantic Ocean. *J. Climate*, **25**, 6594–6609, <https://doi.org/10.1175/JCLI-D-11-00617.1>.
- , and Coauthors, 2018: The third atmospheric scientific experiment for understanding the Earth–atmosphere coupled system over the Tibetan Plateau and its effects. *Bull. Amer. Meteor. Soc.*, **99**, 757–776, <https://doi.org/10.1175/BAMS-D-16-0050.1>.
- , X. Zhou, J. Chen, G. Liu, and S. Nan, 2019: Global climate effects of summer Tibetan Plateau. *Sci. Bull.*, **64**, 1–3, <https://doi.org/10.1016/j.scib.2018.11.019>.